Sensors and Materials, Vol. 37, No. 11 (2025) 4853–4870
MYU Tokyo

S & M 4218

Improved Diamagnetic Levitation Structure and Its Application in Vibration Energy Harvester

Shuang Du,[1] Xia Li,[1] Zhigang Jia,[1] Zhiyong Pang,[1] Kean C Aw,[2] and Yufeng Su[1*]

[1]School of Mechanical and Power Engineering, Zhengzhou University, Zhengzhou 450001, China
[2]Department of Mechanical and Mechatronics Engineering, University of Auckland, Auckland 1010, New Zealand

(Received July 31, 2025; accepted September 22, 2025)

Keywords: diamagnetic levitation, levitation characteristics, magnetism, vibration energy harvester, output performance

In this paper, an array of permanent magnets is proposed as a floating magnet to enhance the levitation characteristics of the diamagnetic levitation structure. Experimental results show that the maximum steady levitation gap of the diamagnetic levitation structure can be increased by 80.21% with the new floating magnet, and the axial size of the diamagnetic levitation structure can be reduced by up to 39.73%. A prototype of a vibration energy harvester based on the diamagnetic levitation structure was constructed. The experimental results show that when the external excitation frequency is 4.8 Hz and the amplitude is 6 mm, the maximum effective voltage of the vibration energy harvester is 1663 mV. Compared with the original structure, the output performance of the vibration energy harvester is improved by 33.87%. This study shows that using this permanent magnet array as a floating magnet not only improves the levitation characteristics of the diamagnetic levitation structure, but also enhances the output performance of the vibration energy harvester.

1. Introduction

Since the Dutch scientist Anton Brugmans discovered diamagnetism in 1778,[1] the research and application of diamagnetism have been continuously deepening. In 1939, Braunbek verified the diamagnetism of graphite and bismuth,[2] successfully achieving their suspension in a strong electromagnetic field. In 2004, Cansiz and Hull conducted the first experimental study of diamagnetic levitation.[3] With the development of manufacturing processes, researchers have found that pyrolytic graphite sheets have strong diamagnetism. Diamagnetically stable levitation can be achieved at room temperature by pyrolytic graphite sheets.[4]

Owing to the advantages of noncontact and low energy loss, diamagnetic levitation technology is widely used in the fields of sensors,[5,6] actuators,[7] and energy harvesters.[8,9] Wang *et al.*[10] designed a diamagnetic levitation based inertial sensor. The sensor has excellent sensitivity and low frequency response achieved by combining the diamagnetic levitation structure with an optical displacement transducer. Xu *et al.*[11] proposed an inclination sensor

*Corresponding author: e-mail: yufengsu@zzu.edu.cn
https://doi.org/10.18494/SAM5861

ISSN 0914-4935

based on diamagnetic levitation with a simple structure, high accuracy, and no power supply. Gao *et al.*[12] studied a novel bistable vibration energy harvester using the diamagnetic levitation mechanism and demonstrated the good compatibility between the low-frequency energy harvester and the diamagnetic levitation structure. In our previous studies,[13,14] we have used this diamagnetic levitation structure to harvest vibration and airflow energy from the environment. Although the energy harvester can achieve higher output performance by utilizing the noncontact nature of the diamagnetic levitation structure, the levitation space of the diamagnetic levitation structure limits the output performance of the energy harvester.

In this paper, we propose a permanent magnet array as the floating magnet to optimize the diamagnetic levitation structure and enhance its levitation characteristics. By increasing the diamagnetic force on the floating magnet, we can obtain a new floating magnet structure that increases the maximum steady levitation gap of the diamagnetic levitation structure. By decreasing the magnetic force of the upper and lower magnets on the floating magnet, we realized a new floating magnet structure that reduces the axial dimension of the diamagnetic levitation structure. While ensuring that the maximum steady levitation gap increases, the output performance of the vibration energy harvester with the new floating magnet is enhanced by increasing the number of induction coils. This floating magnet structure can be applied to electromagnetic actuators and sensors based on the diamagnetic levitation structure to improve their operating characteristics.

2. Theoretical Analysis

2.1 Diamagnetic levitation structure

The diamagnetic levitation structure consists of an upper magnet, an upper highly oriented pyrolytic graphite (HOPG) sheet, a floating magnet, a lower HOPG sheet, and a lower magnet. The 3D model and experimental setup of the diamagnetic levitation structure are shown in Figs. 1(a) and 1(b), respectively. The diamagnetic forces generated by the upper and lower HOPG sheets provide an axial balancing force for the floating magnet. The magnetic forces of the upper and lower magnets balance the gravitational force of the floating magnet and provide a radial balancing force for the floating magnet.

The original structure has a single cylindrical magnet as a floating magnet, as shown in Fig. 2(a). The new floating magnet is an array of permanent magnets, which is composed of a concentric ring-shaped magnet encircling a cylindrical magnet, and the magnetization directions of the circular and cylindrical magnets are opposite, as shown in Fig. 2(b). The levitation characteristics of the diamagnetic levitation structure were analyzed using these two magnets as the floating magnets.

2.2 Levitation characteristic analysis

When a levitating magnet is stably levitating, the axial potential energy of the levitating magnet can be given as

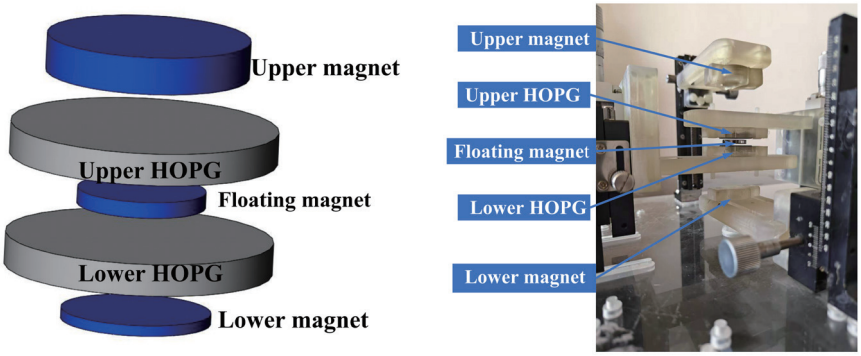

(a) (b)

Fig. 1. (Color online) Diamagnetic levitation structure: (a) 3D model and (b) experimental setup.

(a) (b)

Fig. 2. (Color online) (a) Cylindrical magnet and (b) array of permanent magnets.

$$U = -M\left\{\left(B_{U_0} - B_{L_0}\right) + \left[\left(B_U - B_L\right)' - \frac{mg}{M}\right]z + \frac{1}{2}(B_U - B_L)''z^2 + \cdots\right\} + C_Z Z^2 + C_r Z^2, \quad (1)$$

where $\boldsymbol{M}$ is the magnetic dipole moment of the floating magnet and $\boldsymbol{B_U}$ and $\boldsymbol{B_L}$ are the flux densities of the upper and lower magnets, respectively. m is the weight of the floating magnet and z is the position of the floating magnet from the zero potential energy surface. C_Z is the axial diamagnetic influence coefficient and C_r is the radial diamagnetic influence coefficient. When the floating magnet is in a stable levitating position, the gradient of the magnetic field can be given as

$$\left(B_U - B_L\right)' = \frac{mg}{M}. \quad (2)$$

At this point, the vertical and horizontal stabilities of the diamagnetic levitation structure can be given as follows:

$$K_{Vertical} \equiv C_Z - \frac{1}{2}M\left(B_U - B_L\right)'' > 0, \quad (3)$$

$$K_{Horizontal} \equiv C_r + \frac{1}{4}M\left[\left(B_U - B_L\right)'' - \frac{m^2 g^2}{2M^2\left(B_{U_0} - B_{L_0}\right)}\right] > 0. \tag{4}$$

After the floating magnet deviates from its equilibrium position along the radial direction, the upper and lower magnetic forces can be decomposed into an axial component and a horizontal component. The horizontal recovery force on the floating magnet can be given as

$$F_H = F_{hU} + F_{hL}. \tag{5}$$

The direction of the horizontal recovery force is opposite to the displacement of the floating magnet, so that the floating magnet can return to its equilibrium position.

Figure 3 shows the force variation of the floating magnet under axial external force deviating from the equilibrium position. In Fig. 3, $\Delta \boldsymbol{F}_1$ and $\Delta \boldsymbol{F}_2$ are respectively the variations in magnetic and diamagnetic forces after the floating magnet is displaced along the axial direction. The condition for the diamagnetic levitation structure to achieve axial dynamic equilibrium is given as

$$\left|\Delta F_2\right| > \left|\Delta F_1\right|. \tag{6}$$

The direction of the combined force of $\Delta \boldsymbol{F}_1$ and $\Delta \boldsymbol{F}_2$ is opposite to the direction of the displacement, causing the floating magnet to return to the equilibrium position. The floating

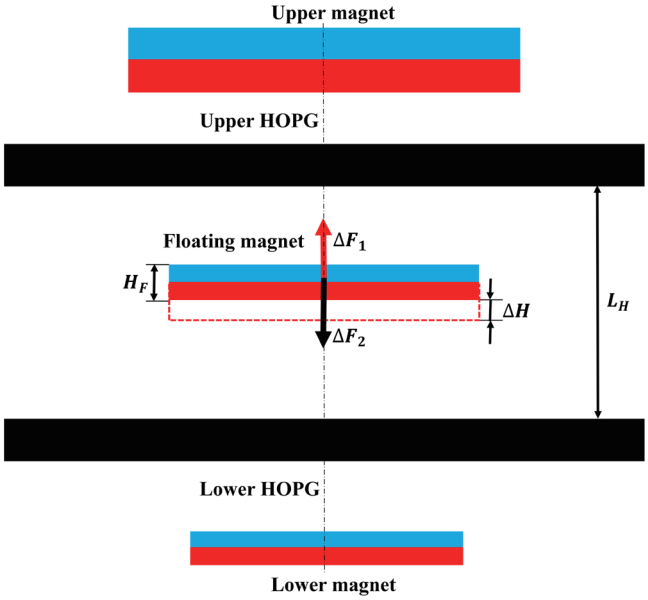

Fig. 3. (Color online) Force variation of the floating magnet when it undergoes axial offset.

magnet is considered to be in a steady levitation space if Eq. (6) is satisfied at any position between two HOPG sheets. There exists a maximum $L_{H_{max}}$ in the steady levitation space. The steady levitation gap of the diamagnetic levitation structure can be given as

$$L_G = L_H - H_F \,, \tag{7}$$

where H_F is the thickness of the floating magnet. The larger the steady levitation space, the higher the stability and environmental adaptability of the diamagnetic levitation structure, which also helps improve the output performance.

2.3 Magnetic and diamagnetic force analysis

The equivalent current method is used to calculate the magnetic force applied to the floating magnet. The equivalent current model of the cylindrical magnet is shown in Fig. 4. The annular region enclosed by the red solid line is the boundary current loop L with a width of dz. The axial magnetic force $\boldsymbol{F_z}$ to which the floating magnet is subjected is generated by the radial magnetic induction intensity $\boldsymbol{B_r}$ of the upper and lower magnets, and the radial magnetic force $\boldsymbol{F_r}$ is generated by the axial magnetic induction intensity $\boldsymbol{B_z}$ of the upper and lower magnets. The magnetic forces of the upper and lower magnets on a single current loop at height z on the floating magnet can be given as follows:

$$f_z = nIdz\oint dL \times B_r\left(r,z\right), \tag{8}$$

$$f_r = nIdz\oint dL \times B_z\left(r,z\right). \tag{9}$$

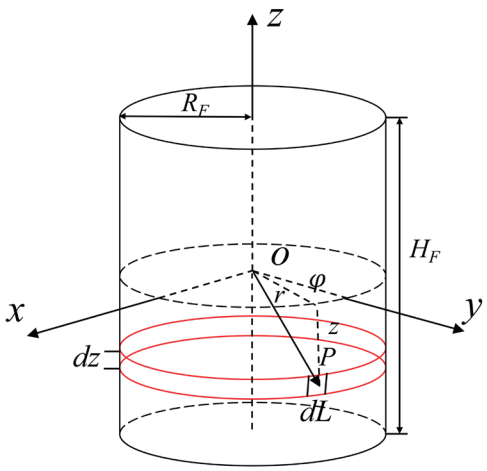

Fig. 4. (Color online) Equivalent current model of the cylindrical magnet.

By integrating a single current loop in the axial direction, we can express the magnetic force on the floating magnet as follows:

$$F_z = nI\int_{\frac{H}{2}+L}^{\frac{H}{2}+L+H_F} dz \oint dL \times B_r(r,z), \tag{10}$$

$$F_r = nI\int_{\frac{H}{2}+L}^{\frac{H}{2}+L+H_F} dz \oint dL \times B_z(r,z), \tag{11}$$

where H is the thickness of the upper and lower magnets and L is the distance between the magnets.

When the equivalent current method is used to calculate the magnetic force of the new floating magnet, the magnetic force applied to the new floating magnet can be equated to the superposition of the magnetic force of three cylindrical magnets, because there is no need to take into account the current circle inside the magnet,[15] and the equivalent model is shown in Fig. 5. $\boldsymbol{M}$ denotes the magnetization strength of the magnet. Therefore, the expression for calculating the magnetic force of the new floating magnet can be written as

$$F_z = nI\int_{\frac{H}{2}+L}^{\frac{H}{2}+L+H_F} dz \oint dL \times \left(B_{r_1}(r,z) + 2B_{r_2}(r,z)\right), \tag{12}$$

$$F_r = nI\int_{\frac{H}{2}+L}^{\frac{H}{2}+L+H_F} dz \oint dL \times \left(B_{z_1}(r,z) + 2B_{z_2}(r,z)\right). \tag{13}$$

The diamagnetic force exerted on the floating magnet can be given as

$$dF = M \cdot \nabla(B)dv, \tag{14}$$

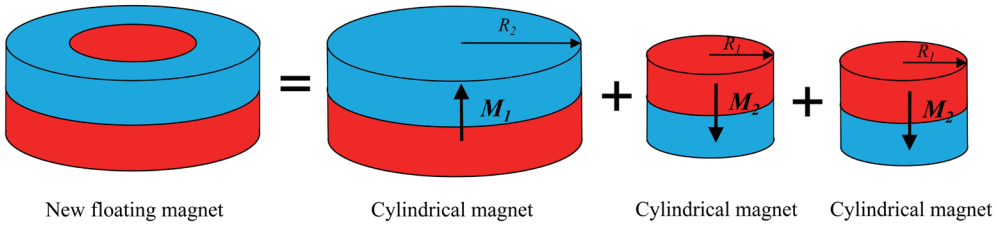

Fig. 5. (Color online) Equivalent model of the new floating magnet.

where $\boldsymbol{B}$ is the magnetic induction intensity of the floating magnet and $\boldsymbol{M}$ is the magnetization of the pyrolytic graphite plate, which can be expressed as

$$M = \frac{\chi_m B}{\mu_0 (1+\chi_m)} = \frac{\chi_m B}{\mu_0}, \tag{15}$$

where χ_m is the magnetic susceptibility of the pyrolytic graphite plate, which has a very small value. According to the Gauss scattering theorem, the diamagnetic force of the floating magnet can be obtained as

$$\begin{cases} F_r = \dfrac{\chi_m}{2\mu_0} \oiint \|B\|^2 n_r \cdot ds, \\ F_z = \dfrac{\chi_m}{2\mu_0} \oiint \|B\|^2 n_z \cdot ds, \end{cases} \tag{16}$$

where $\boldsymbol{n_r}$ and $\boldsymbol{n_z}$ are the radial and axial unit vectors, respectively, and ds is the surface area unit on the pyrolytic graphite sheet.

3. Simulation Analysis

3.1 Force analysis

The structural parameters of the diamagnetic levitation structure are presented in Table 1. The finite element simulation model was built in COMSOL. From Eqs. (12) and (13), it can be seen that when the radius of the cylindrical magnet inside the new floating magnet varies, the magnetic force on the new floating magnet also varies. The volume proportion of the cylindrical magnet within the new floating magnet is written as

Table 1
Structural parameters of the diamagnetic levitation structure.

Symbol	Parameter	Value
$\boldsymbol{B}$	Residual magnetic flux density	1.45 T
ρ	Magnet density	7.5 g/cm^3
D_U	Upper magnet diameter	20 mm
H_U	Upper magnet thickness	6.5 mm
D_F	Floating magnet diameter	18 mm
H_F	Floating magnet thickness	3 mm
D_L	Lower magnet diameter	18 mm
H_L	Lower magnet thickness	2 mm
D_H	HOPG diameter	25 mm
H_H	HOPG thickness	5.5 mm
D_1	Cylindrical magnet inside the new floating magnet diameter	11 mm

$$\eta = \frac{V_1}{V_{all}}, \tag{17}$$

where V_1 is the volume of the cylindrical magnet within the new floating magnet and V_{all} is the volume of the new floating magnet. Figures 6(a) and 6(b) show the change in magnetic force on the new floating magnet when η and the distance between the magnets vary. The axial magnetic force on the floating magnet decreases as the distance between the magnets increases. When the distance between the magnets is constant, with a gradual increase in η, the upper and lower magnetic forces on the new floating magnet decrease first, and when η exceeds 45%, the direction of the magnetic force changes, and the magnetic force gradually increases with η. From the simulation results, the overall direction of magnetization of the new floating magnet changes with the increase in η. However, for the diamagnetic levitation structure to be horizontally stable, the direction of magnetization of the floating magnet has to be the same as that of the upper and lower magnets.[9] Therefore, when η exceeds 45%, it is necessary to reverse the new floating magnet, as shown in Fig. 7.

According to Eq. (16), the diamagnetic force on the floating magnet is determined by the square of the magnetic flux density $\boldsymbol{B}^2$, which $\boldsymbol{B}^2$ can be given as

$$B^2 = {B_z}^2 + {B_r}^2 . \tag{18}$$

The distribution of $\boldsymbol{B}^2$ in the horizontal plane with an axial distance of 0.5 mm from the upper surface of the cylindrical magnet and the new floating magnet is shown in Fig. 8. From Fig. 8, it can be seen that the square of the magnetic flux density $\boldsymbol{B}^2$ of the new floating magnet is generally much larger than that of the cylindrical magnet in the same plane. This means that when the diamagnetic material is in this plane, the new floating magnet is subjected to a larger diamagnetic force than the cylindrical magnet.

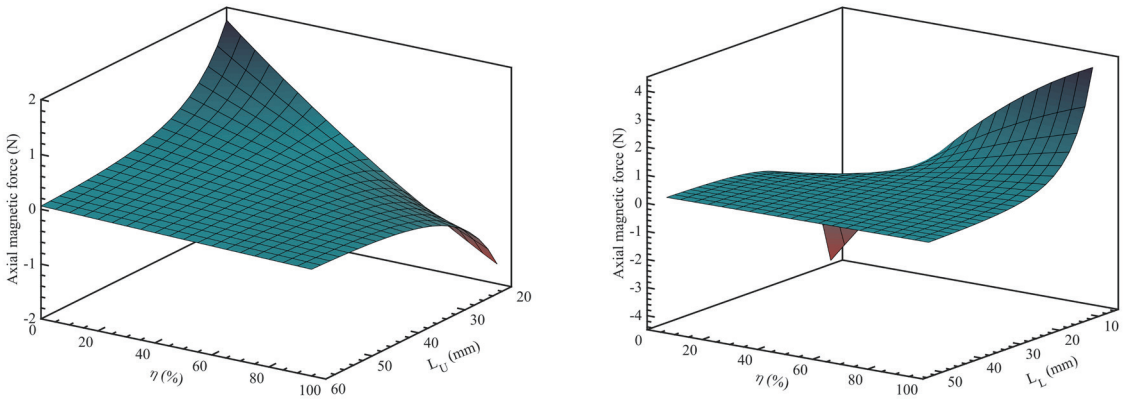

(a) (b)

Fig. 6. (Color online) Axial magnetic force on the new floating magnet varies with the volume share of the cylindrical magnet and the distance between the magnets: (a) upper and (b) lower magnetic forces.

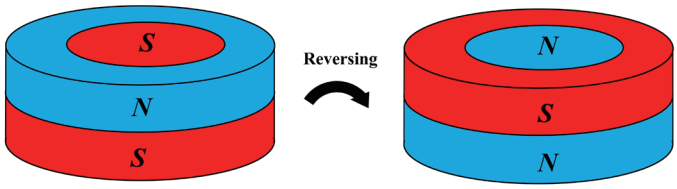

Fig. 7. (Color online) Reversal of the new floating magnet to maintain the radial stability of the diamagnetic levitation structure.

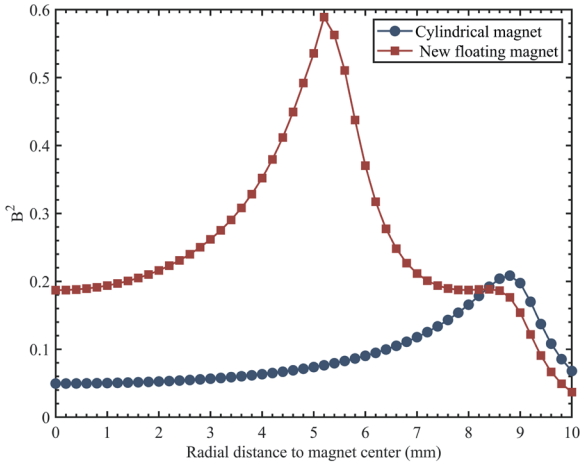

Fig. 8. (Color online) Distribution of the magnetic flux density $\boldsymbol{B}^2$ in the horizontal plane at a distance of 0.5 mm from the upper surface of the magnet.

Figure 9 shows the change in diamagnetic force on the new floating magnet when η and the distance between the new floating magnet and HOPG vary. As the distance between the new floating magnet and HOPG increases, the diamagnetic force applied to the floating magnet decreases. When the distance between the magnet and HOPG is constant, the diamagnetic force on the new floating magnet increases and then decreases as η continues to increase. The simulation results show that the new floating magnet is subjected to a greater diamagnetic force than the cylindrical floating magnet.

4. Experimental Verification

4.1 Experiments on levitation characteristics

The experimental platform is shown in Fig. 10. The structural parameters are listed in Table 1. The upper and lower magnets and the upper and lower HOPG sheets are fixed to an acrylic base plate through several axially adjusting tables and 3D printed connectors, where the material

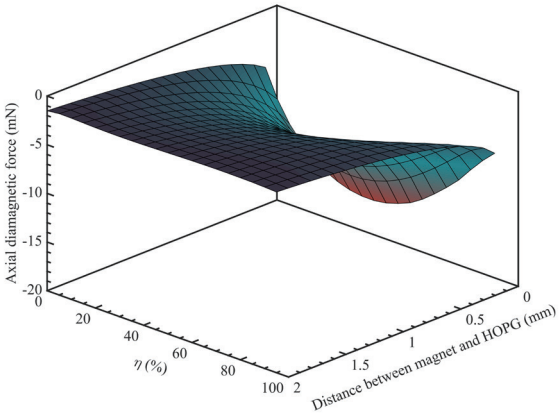

Fig. 9. (Color online) Axial diamagnetic force on the new floating magnet varies with the volume share of the cylindrical magnet and the distance between the new floating magnet and HOPG.

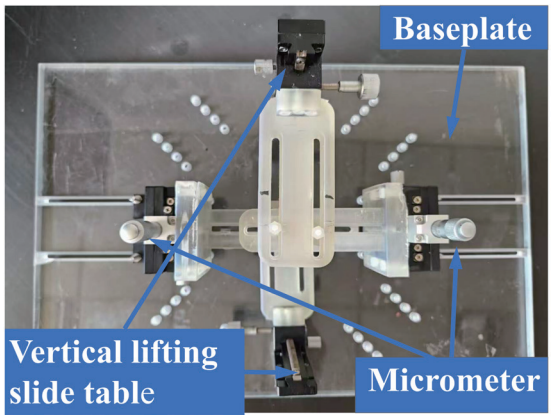

Fig. 10. (Color online) Experimental platform of the diamagnetic levitation structure.

of choice for 3D printing is nonmagnetic photosensitive resin. The distance between the upper and lower HOPG sheets can be adjusted using micrometers on the adjusting table. The spacing between the upper and lower magnets, and the floating magnet is adjusted by the vertical lifting slide. The upper magnet, upper HOPG sheet and lower magnet are adjusted to measure the maximum levitation gap and the maximum axial dimension of the diamagnetic levitation structure. Owing to experimental constraints, this experiment disregards the effects of environmental factors such as temperature on magnets. The experimental temperature is set at 30 °C.

A mathematical model is set up in MATLAB to calculate the theoretical value of the maximum steady levitation gap of the diamagnetic levitation structure. In the experiments, the vertical lifting slide was used to adjust the distance between the upper and lower magnets, and the floating magnet so that the floating magnet could be stably levitated. The maximum steady levitation gap is calculated on the basis of the axial stability of the diamagnetic levitation structure. Micrometers were used to continuously increase the distance between the upper and

lower HOPG sheets until the floating magnet did not return to the equilibrium position at the maximum axial displacement.

Figures 11(a) and 11(b) show the changes in the maximum steady levitation gap of the diamagnetic levitation structure when the volume share η of the cylindrical magnet within the new floating magnet varies. There is good agreement between the simulation and experimental results. In Fig. 11(a), when η = 0%, i.e., when the cylindrical floating magnet is used, the maximum steady levitation gap obtained from the experiment is 1.92 mm, as shown in Fig. 12(a). When η = 0–40%, the experimental value of the maximum steady levitation gap increases from 1.92 to 3.46 mm as η increases. In Fig. 11(b), when η = 45%, both simulation and experimental results show that the new floating magnet cannot be stably levitated because the magnetic force to which it is subjected is small. When η = 50–100%, the experimental value of the maximum steady levitation gap decreases from 2.89 to 1.92 mm as η increases. According to the experimental results, when η = 40%, the maximum steady levitation gap of 3.46 mm is achieved, as shown in Fig. 12(b).

The axial dimension of the diamagnetic levitation structure reflects the overall size of the diamagnetic levitation structure. The axial dimension of the diamagnetic levitation structure is maximum when the steady levitation gap is maximum. The steady levitation gap decreases as the distance between the magnets decreases. When the steady levitation gap is 0 mm, the axial dimension is minimum.

Figures 13(a) and 13(b) show the changes in the maximum axial dimension of the diamagnetic levitation structure when the volume share η of the cylindrical magnet within the new floating magnet varies. The results of the experiment agree with those of the simulation. In Fig. 13(a), when η = 0–40%, the experimental value of the maximum axial dimension decreases from 161.02 to 117.76 mm as η increases. In Fig. 13(b), when η = 50–100%, the experimental maximum axial dimension increases from 97.04 to 161.02 mm as η increases. According to the experimental

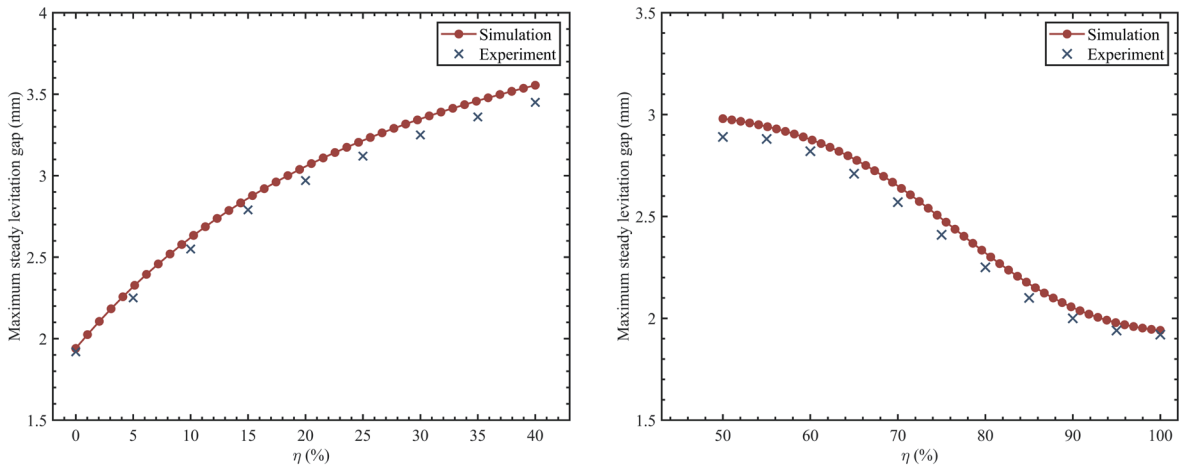

Fig. 11. (Color online) Maximum steady levitation gap of the diamagnetic levitation structure varies with the volume share η of the cylindrical magnet within the new floating magnet: (a) η =0–40% and (b) η = 45–100%.

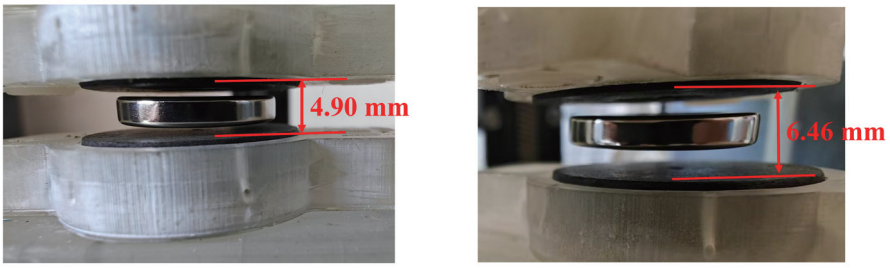

(a) (b)

Fig. 12. (Color online) (a) Cylindrical and (b) new floating magnets.

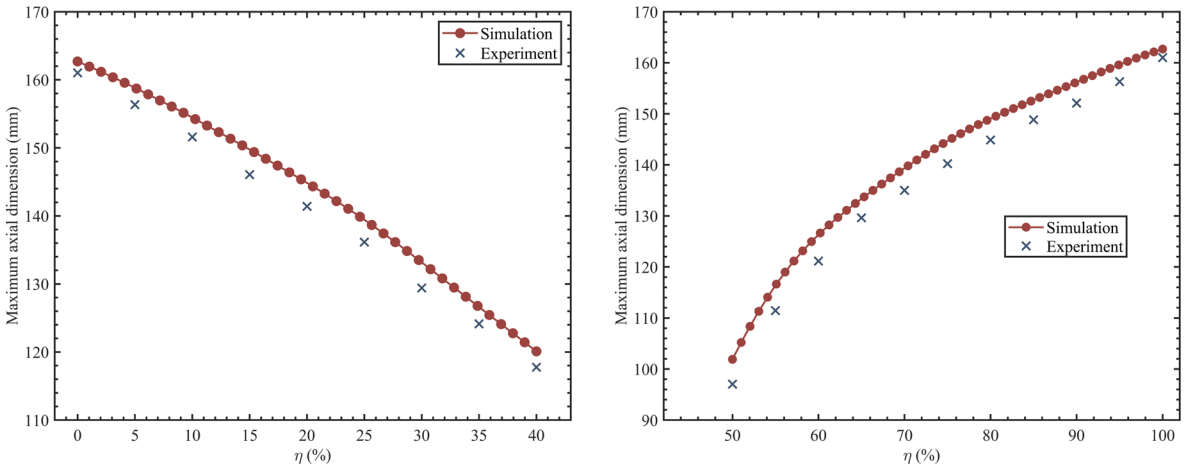

Fig. 13. (Color online) Maximum axial dimension of the diamagnetic levitation structure varies with the volume share η of the cylindrical magnet within the new floating magnet: (a) η = 0–40% and (b) η = 45–100%.

results, when η = 50%, the maximum axial dimension is achieved with a minimum value of 97.04 mm.

When using the new floating magnet, the experimental results show that the maximum steady levitation gap of the diamagnetic levitation structure increases by 80.21% and the maximum axial dimension of the diamagnetic levitation structure decreases by up to 39.73%. The maximum relative error between the experimental and simulation results is 3.11%, and the main source of the error is the difference between the actual magnetic field strength of the magnet and the theoretical value. The experimental results of levitation characteristics illustrate that the use of the new floating magnet can not only increase the maximum steady levitation gap of the diamagnetic levitation structure, but also reduce the size of the diamagnetic levitation structure.

4.2 Output performance experiment

Owing to the noncontact nature of the diamagnetic levitation structure, it has a high application prospect in the field of energy harvesting. In this study, a vibration energy harvester based on the diamagnetic levitation structure was fabricated to test the effect of the new floating magnet on energy harvesting performance.[14,16,17] The vibration energy harvester prototype is shown in Fig. 14(a). The induction coils are fixed to the upper and lower HOPG sheets, and their parameters are shown in Table 2. When the floating magnet moves in the horizontal direction, the change in magnetic field generates an induced voltage inside the induction coils, thus enabling vibration energy harvesting.[18,19] The experimental platform is shown in Fig. 14(b). The horizontal excitation received by the prototype is provided by the vibration exciter (LT-50-ST250; ECON). The parameters of the harmonic excitation generated by the exciter are adjusted by the vibration controller (VT9002; ECON). The power amplifier (LSA-V5000A; ECON) provides the required power to the exciter during operation. The oscilloscope (MDO34; Tektronix) can measure the voltage waveform generated by the energy harvester prototype during the experiments. A computer can process the signals received by the oscilloscope and interface with the vibration controller to adjust the parameters of the harmonic excitation.

The frequency of the vibration exciter was adjusted to be 4.8 Hz and the amplitude to be 6 mm. When the volume share η of the cylindrical magnet within the new floating magnet varies, the output voltage of a single induction coil of the vibration energy harvester changes, as shown

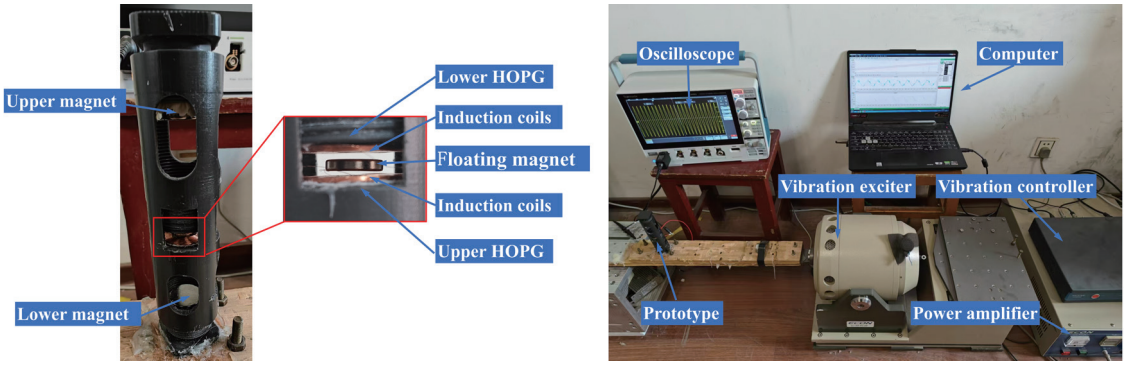

(a) (b)

Fig. 14. (Color online) Experimental setup of the vibration energy harvester: experimental (a) prototype and (b) platform.

Table 2
Parameters of induction coils.

Parameter	Value
Material	Cu
Outer diameter	24.5 mm
Inner diameter	5 mm
Wire diameter	0.06 mm
Number of coil layers	12
Internal resistance	720 Ω

in Fig. 15. In Fig. 15, when η = 0–40%, the output voltage of a single induction coil decreases from 619.43 to 398.81 mV as η increases. When η = 50–100%, the experimental value of the maximum axial dimension increases from 296.98 to 619.43 mV as η increases. The output voltage of the induction coil is both related to the flux density distribution of the floating magnet and affected by the distance between the induction coil and the floating magnet.

According to the experimental results, compared with the cylindrical floating magnet, the output voltage of a single induction coil of the vibration energy harvester with new floating magnets decreases. However, since the maximum steady levitation gap of the energy harvester increases with the use of new floating magnets, the output performance of the energy harvester can be improved by increasing the number of coils. The thickness of a single induction coil is 0.6 mm. When the cylindrical floating magnet is used, only one induction coil can be fixed on the upper and lower HOPG sheets. The actual maximum steady levitation gap of the energy harvester is 0.72 mm. When using the new floating magnet with η = 40%, two induction coils can be fixed on the upper and lower HOPG sheets. In this case, the actual maximum steady levitation gap of the energy harvester is 1.06 mm. Using these two floating magnets separately, we obtained the output voltage waveform of the vibration energy harvester as shown in Fig. 16. In Fig. 16, when using the cylindrical and new floating magnets, the effective output voltages of the vibration energy harvester are 1.24 and 1.66 V, respectively. The output performance of the vibration energy harvester is improved by 33.87% with the new floating magnet. Concurrently, the stable output voltage waveforms demonstrate that the vibration energy harvester exhibits favorable horizontal vibration stability. When using the cylindrical and new floating magnets, the energy harvester's output powers without load connection are 1067.8 and 956.8 μW, and power densities are 10.77 and 13.20 W/m^3 respectively. The power density of the vibration energy harvester is improved by 22.56% with the new floating magnet. A comparison of performance metrics of the vibrational energy harvester before and after improvement is shown in Table 3.

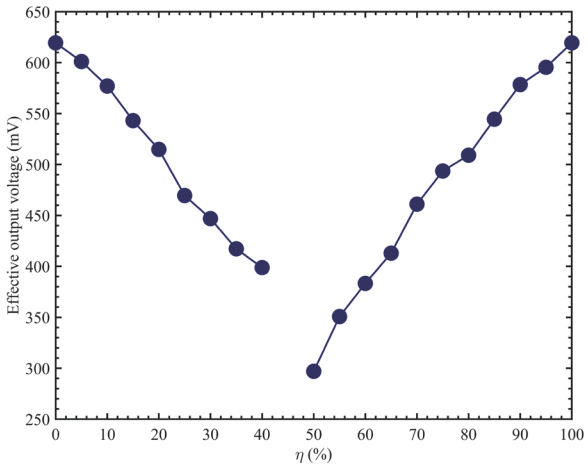

Fig. 15. (Color online) The output voltage of a single induction coil of the vibration energy harvester varies with the volume share η of the cylindrical magnet within the new floating magnet.

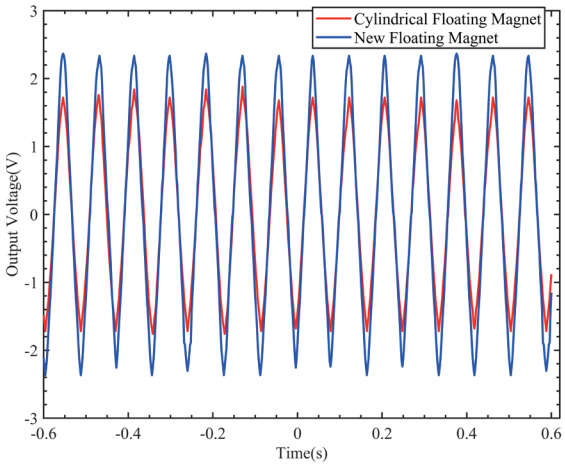

Fig. 16. (Color online) Waveforms of the output voltage of the vibration energy harvester with the cylindrical and new floating magnets with η = 40%.

Table 3
Performance metrics of the vibration energy harvester with different floating magnets.

Performance metric	Cylindrical floating magnet	New floating magnet
Number of induction coils	2	**4**
Actual maximum steady levitation gap (mm)	0.72	**1.06**
Effective output voltage (V)	1.24	**1.66**
Output power (μW)	**1067.8**	956.8
Power density (W/m^3)	10.77	**13.20**

5. Conclusions

In this paper, a new floating magnet structure is proposed to improve the performance of the diamagnetic levitation structure. The levitation characteristics of the improved diamagnetic levitation structure and the output performance of the vibration energy harvester are investigated through simulation analysis and experimental verification. The optimal structural dimensions of the new floating magnet are determined by parametric analysis. In summary, there are three enhancements to the diamagnetic levitation structure when using the new floating magnet:

(1) The maximum steady levitation gap of the diamagnetic levitation structure improves. The maximum steady levitation gap of the diamagnetic levitation structure with the new floating magnet is 3.46 mm, which is 80.21% higher than that of the original structure.
(2) The size of the diamagnetic levitation structure decreases. The minimum axial dimension of the improved diamagnetic levitation structure is 97.04 mm, and the axial dimension can be reduced by up to 39.73% compared with the original structure.
(3) The vibration energy harvester based on the improved diamagnetic levitation structure can increase the output performance by 33.87% and the power density by 22.56%.

Both simulation analyses and experiments strongly demonstrate the great potential of the new floating magnet in improving the environmental adaptability and energy harvesting

efficiency of the diamagnetic levitation structure. In the future, we shall conduct further research on the multi-axis vibration stability of the vibration energy harvester when subjected to vibrations from multiple directions simultaneously and test the long-term reliability of vibration energy harvesters in complex environments.

Acknowledgments

This work was supported by the National Natural Science Foundation of China under Grant No. U1904169, the China Scholarship Council under Grant No. 202107045007, and the Henan Province Science and Technology Research Project under Grant No. 232102220005.

References

1 S. Pelloni, P. Lazzeretti, and R. Zanasi: J. Phys. Chem. A **113** (2009) 14465. https://dx.doi.org/10.1021/jp903859k
2 W. Braunbek: Z. Physik **112** (1939) 764. https://doi.org/10.1007/BF01339980
3 A. Cansiz and J. R. Hull: IEEE Trans. Magn. **40** (2004) 1636. https://ieeexplore.ieee.org/document/1298938
4 X. Chen, S. K. Ammu, K. Masania, P. G. Steeneken, and F. Alijani: Adv. Sci. **9** (2022) 2203619. https://doi.org/10.1002%2Fadvs.202203619
5 Y. Wang, Y. P. Xu, L. Yang, J. Zhou, J. Mahfoud, and C. W. Jin: Measurement **245** (2025) 116651. https://doi.org/10.1016/j.measurement.2025.116651
6 X. F. Chen, N. Kothari, A. Keşkekler, P. G. Steeneken, and F. Alijani: Sens. Actuators, A **330** (2021) 112842. https://doi.org/10.1016/j.sna.2021.112842
7 W. Liu, W. P. Zhang, and W. Y. Chen: J. Magn. Magn. Mater. **492** (2019) 165634. https://doi.org/10.1016/j.jmmm.2019.165634
8 B. B. Wang, L. Zhang, B. Y. Li, K. C. Aw, and Y. F. Su: IEEE Sens. J. **24** (2024) 29760. https://doi.org/10.1109/JSEN.2024.3442202
9 H. Shao, X. Li, S. H. Chang, K. C. Aw, and Y. F. Su: IEEE Sens. J. **23** (2023) 11469. https://doi.org/10.1109/JSEN.2023.3265961
10 Q. Wang, X. F. Ren, S. M. Jiao, X. Z. Lei, S. Zhang, H. F. Liu, P. Luo, and L. C. Tu: Sens. Actuators, A **312** (2020) 112122. https://doi.org/10.1016/j.sna.2020.112122
11 Y. P. Xu, Q. Q. Jiang, K. Yang, J. Zhou, and Q. T. Guo: Sens. Actuators, A **343** (2022) 113686. https://doi.org/10.1016/j.sna.2022.113686
12 Q. H. Gao, W. M. Zhang, H. X. Zou, W. B. Li, Z. K. Peng, and G. Meng: IEEE Trans. Magn. **53** (2017) 1. https://doi.org/10.1109/TMAG.2017.2732943
13 H. Shao, F. Bian, L. Zhang, J. X. Zhang, K. C. Aw, and Y. F. Su: IEEE Sens. J. **23** (2023) 13942. https://doi.org/10.1109/JSEN.2023.3275974
14 J. X. Zhang, H. Shao, L. Zhang, D. P. Liu, K. C. Aw, and Y. F. Su: Appl. Phys. A **130** (2024) 92. https://doi.org/10.1007/s00339-023-07264-y
15 Y. P. Xu, Y. Zhang, J. Zhou, and C. W. Jin: Chin. J. Mech. Eng. (Engl. Ed.) **37** (2024) 67. https://doi.org/10.1186/s10033-024-01053-1
16 X. Y. Xiang, S. J. Liu, Q. Yang, H. Shen, and R. J. Song: Energy **322** (2025) 135589. https://doi.org/10.1016/j.energy.2025.135589
17 K. A. Omoteso, T. O. Roy-Layinde, and U. H. Diala: Int. J. Non-Linear Mech. **170** (2025) 104989. https://doi.org/10.1016/j.ijnonlinmec.2024.104989
18 X. Wang, Y. Zhang, S. H. Xue, T. Wang, G. Q. Guoqiang, X. Y. Mao, and C. J. Lu: Mech. Syst. Sig. Process. **199** (2023) 110478. https://doi.org/10.1016/j.ymssp.2023.110478
19 D. N. Hao, L. J. Kong, Z. T. Zhang, W. H. Kong, A. M. Tairab, X. Lou, A. Ahmed, and Y. W. Yang: Sustainable Energy Technol. Assess. **57** (2023) 103184. https://doi.org/10.1016/j.seta.2023.103184

About the Authors

Shuang Du received his B.S. degree in Mechanical and Electronic Engineering from China Jiliang University, Hangzhou, China, in 2023. He is currently pursuing his master's degree in mechanical engineering from Zhengzhou University, Zhengzhou, China. His research interests include vibration and airflow energy harvesters utilizing diamagnetic levitation. (2821565526@qq.com)

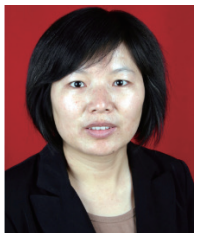

Li Xa received her B.S., M.S., and Ph.D. degrees in mechanical engineering from Harbin Institute of Technology in 1996, 2000, and 2007, respectively. She is an associate professor at the School of Mechanical Engineering, Zhengzhou University. Her research interests include piezoelectric energy harvesting technology in vehicles, ultrasonic molding technology for microdevices, and off-highway vehicle design and analysis. (Lx2007@zzu.edu.cn)

Zhigang Jia received his B.S. and M.S. degrees in measuring technology and instruments from Zhengzhou University and Xiamen University, in 2020 and 2009, respectively, and his Ph.D. degree in nanomechanics from Tohoku University in 2015. He is a lecturer at the School of Mechanical and Power Engineering, Zhengzhou University, Zhengzhou, China. His research interests include developing devices and systems in the area of precision and nanomanufacturing and metrology, and optometric correction. (jiazhigang@zzu.edu.cn)

Zhiyong Pang received his B.Sc. degree from Zhengzhou University in 2024 and is currently a master's student at Zhengzhou University. His main research interests include energy harvesters. (ll674@outlook.com)

Kean C Aw received his Engineering Council (U.K.) degree in electrical and electronics engineering from the Tunku Abdul Rahman College, Kuala Lumpur, Malaysia, in 1986, M.Sc. degree in advanced manufacturing systems from Brunel University, London, U.K., in 1998, and Ph.D. degree in applied physics from the University of Science, Penang, Malaysia, in 2002. In 2004, he joined the Department of Mechanical and Mechatronics Engineering, University of Auckland, Auckland, New Zealand, where he is currently a professor. His main research interests include microsystems and the deployment of smart/functional materials and structures. (k.aw@auckland.ac.nz)

Yufeng Su received his B.S. degree in mechatronics and M.S. degree in mechanical design, manufacture, and automation from Shaanxi University of Science and Technology, in 1999 and 2002, respectively, and Ph.D. degree in microelectronics and solid-state electronics from Shanghai Jiao Tong University, Shanghai, China, in 2006. He is currently a professor at the School of Mechanical Engineering, Zhengzhou University, Zhengzhou, China. His research interests include the design and analysis of micro-electromechanical systems (MEMS) devices, electromechanical system control, micro-energy harvesters, and microactuators. (yufengsu@zzu.edu.cn)